Particle Identification using dE/dx in the CTD at ZEUS

Matthew Wing[1]

Transfer report - September 1996

Abstract

The measurement of the rate of loss of energy, dE/dx is an important quantity for the purpose of distinguishing types of particles produced in the ZEUS experiment. To obtain these values, a correction procedure, resulting from both external and internal factors (to the detector), is undertaken. A method of external correction has been applied to all the 1995 data and the possibility of improving the values has been studied. The resulting values can then be used in analyses as a means of particle identification.

[1] University College London

Contents

List of Figures

1 Introduction

This report contains the work that has been done concerning "dE/dx". This is a continuation of work initiated by Julian Shulman. Briefly, the work entails using ionization energy loss measurements, the aforementioned dE/dx, for particle identification. Particles traversing the Central Tracking Detector (CTD) at ZEUS lose energy by ionizing the atoms within the gas in the detector. A raw pulse size is measured, which then has to be converted into a more meaningful and useful quantity. There are many checks that have to be made on the raw pulse and these will be detailed herein. There are also external effects which alter the "true" value of dE/dx, with pressure variations being the most important. These pressure corrections are covered in detail in this report.

Initially, the theory behind ionization energy losses will be outlined and a description of the ZEUS detector will be given. The general description of the ZEUS detector will be short. A more detailed account of the CTD and its relevance to dE/dx measurements is given.

How an average dE/dx value is determined for a track is then discussed in Chapter 5. A track consists of a number of hits within the central tracking detector. The mean of these hits is found, to give a track value for dE/dx. Several ways of finding the mean were looked at and these are compared in the chapter.

How the pressure corrections were computed and the results are the subject of Chapter 6. This chapter also looks at the usefulness of the corrected dE/dx values and their applicability in analyses. The subject of how corrected dE/dx measurements could and have been used in the analysis of D^* production in photoproduction will be briefly discussed in the final chapter. As these will form analysis topics in the coming years, some theoretical details of photoproduction, and how dE/dx measurements are applied will be expounded. The results have already been used in identifying pions in D^* decay and may also be used in identifying electrons in the semi-leptonic decay of the D^* mesons.

2 Ionization Energy Loss

2.1 What is Energy Loss?

The theory of the energy loss of charged particles traversing a medium is well documented [1]. An account of the basic principles is detailed here. For all charged particles, ionization losses dominate over radiation losses except for electrons and positrons at all but the highest attainable energies. These ionization losses are dominated by Coulomb scattering off atomic electrons. There is some scattering from the nucleus but this is a negligible effect since the recoil energy of the nucleus is much smaller because of its greater mass. This theory was put forward in the 1930s by Bethe and Bloch (and others) and is formulated in the Bethe-Bloch equation [2].

2.2 The Bethe-Bloch Formulation

In the computation, it is essential to take into account the binding of electrons to the atoms; therefore, one should consider the system formed by the atom and by the incident particle and then compute the probabilities for the various possible transitions leading to excitation or ionization of the atom. Bethe's formulation was based along these lines using Born's approximation. The original result was updated and went through more accurate calculations [3] and is now given below in its modern form.

For a scalar $spin-0$ boson with charge equal to plus or minus the electron charge, the Bethe-Bloch equation is given by,

$$\frac{-dE}{dx} = \frac{DZ^2 n_e}{\beta^2}\left[\ln\left(\frac{2mc^2\beta^2\gamma}{I}\right) - \beta^2 - \frac{\delta(\gamma)}{2}\right] \tag{1}$$

where x is the distance travelled through the meduim, m is the electron mass, Z is the atomic number and

$$D = \frac{4\pi\alpha^2\hbar^2}{m} = 5.1.10^{-25} MeV cm^2 \tag{2}$$

The other terms are properties of the medium; $\delta(\gamma)$ is a dielectric screening correction which is important for highly relativistic particles; I is the mean ionization potential of the atoms averaged over all electrons, which is given approximately by $I = 10Z$ eV for $Z > 20$; and n_e is the electron density and is given by,

$$n_e = \frac{\rho N_A Z}{A} \tag{3}$$

where N_A is Avogadro's number, ρ is the mass density and A is the atomic weight of the medium.

For $spin - 1/2$ particles the main features of the Bethe-Bloch equation are the same and the effects of the differences small, so can be ignored in this general discussion of ionization energy losses.

The main features of the equation can be seen in figure 1, which shows how $-dE/dx$ varies as a function of momentum for different particles, namely (a) electrons, (b) pions, (c) kaons and (d) protons. This is a theoretical curve for conditions typical to the CTD at ZEUS. The important points to note are the rapid fall in $-dE/dx$ as the velocity increases from zero due to the $1/\beta^2$ factor. Then there is the region of *minimum ionization*, where the curves are at or around their minimum value, which, for example is between 0.3 and 0.4 $GeVc^{-1}$ for a pion. After the region of minimum ionization, β tends towards 1 and the logarithmic factor gives a *relativistic rise* in $-dE/dx$, which can be seen on close inspection of the graph. There are two reasons for this rise: firstly as the velocity increases, the relativistic deformation of the Coulomb field of the incident particle causes the effects of this particle to be felt at larger distances from its geometric path, thereby increasing the upper limit of the impact parameter; and secondly as the momentum increases, the lower limit of the impact parameter decreases due to the uncertainty principle. This relativistic rise then slows down as the screening correction, δ, becomes important. Note also that these features apply only to the three baryons and not to the electron. The electron has a momentum independent value of dE/dx.

Therefore, since the value of dE/dx depends on the velocity of the charged particle, it is possible to distinguish different particles with the same momentum but different masses by a careful measurement of dE/dx. This measurement of dE/dx is is carried out at ZEUS using the CTD.

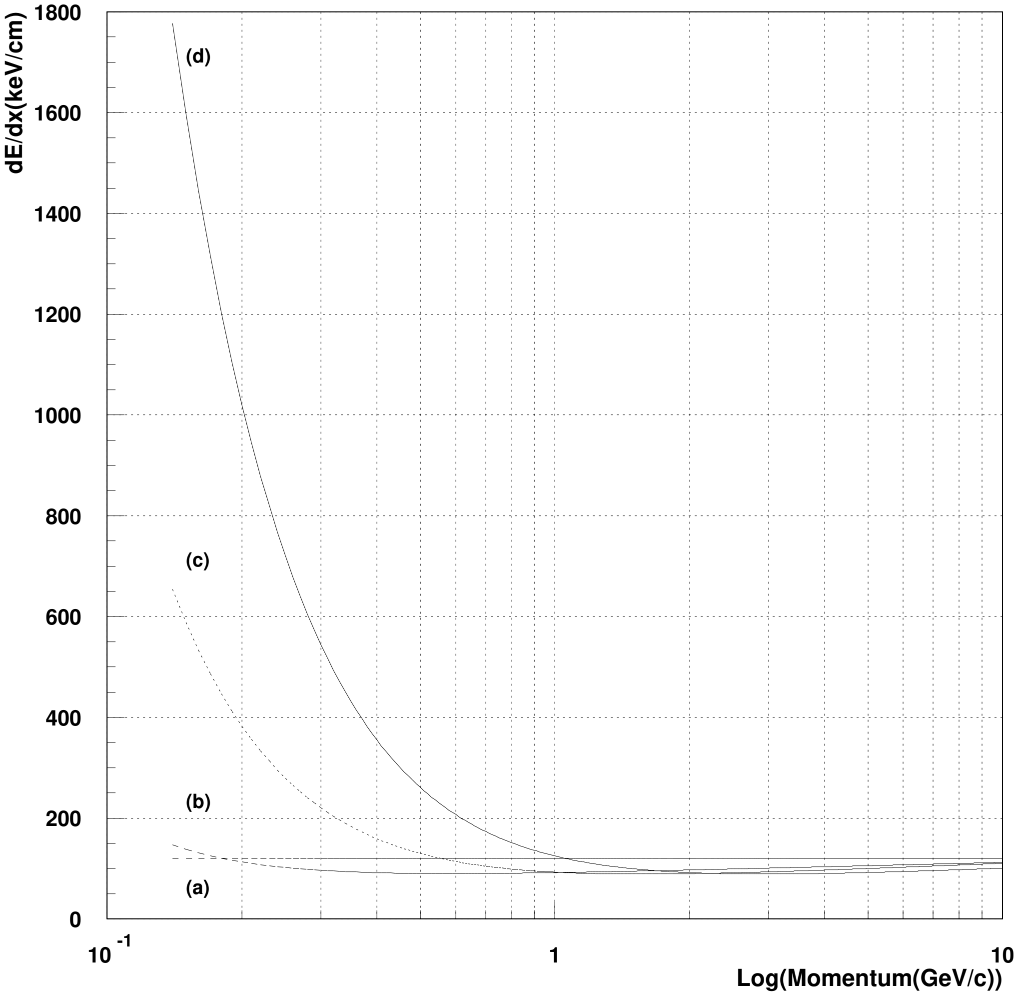

Figure 1: Theoretical Bethe-Bloch curves of dE/dx against momentum on a logaritmic scale for, (a) electrons, (b) pions, (c) kaons and (d) protons.

3 HERA and the Zeus Detector

3.1 Overview of HERA

The Hadron Electron Ring Anlage (HERA) was constructed by DESY (Deutsches Electronen Synchrotron), the German National Particle Physics Laboratory. It is unique amongst particle accelerators in that it is an electron-proton collider. It provides physics with tests of the theory of QCD (Quantum Chromodynamics) and will also (with the proposed luminosity upgrade) investigate Electroweak physics. The accelerator is situated in Hamburg and is 6.3km in circumference. The colliding beams provide a large centre-of-mass energy, $\sqrt{s}$, of 314 GeV. This arises from the beams having an energy of 820 GeV and up to 30 GeV for the proton and electron respectively. This enables the testing of QCD predominantly via studies of Deep Inelastic Scattering (DIS) and photoproduction. There is also the opportunity to search for *exotic* phenomena such as leptoquarks and the supersymmetric analogues of the quarks and leptons. There are two large detectors built for HERA at the north and south interaction points. These are H1 and ZEUS respectively. These detectors measure high-energy jets of up to several hundred GeV with great precision and also measure the scattered lepton. These jets are predominantly in the proton direction as is the scattered lepton at high Q^2, where,

$$Q^2 \equiv -q^2 = (p_f - p_i)^2 \, ; \tag{4}$$

q being the 4-momentum transfer between the interacting particles; p_i the initial and p_f the final momentum of one of the particles. This is due to the large momentum imbalance of the proton and electron. Therefore the detectors are hermetic detectors, with particle detection being possible over the full 360° range except for a small area close to the beam pipe. This briefly outlines HERA and the ZEUS detector, and the latter specifically, will now be discussed.

3.2 The ZEUS Detector

Much of what is said in what follows can be found in more detail in [4]. The detector layout is shown in Fig.(2) and the main features of ZEUS are now expounded. Centred around the beam-pipe is a Central Tracking Detector (CTD). Planar drift chambers, the Forward Tracking Detector (FTD) and the

Rear Tracking Detector (RTD) are positioned at the front and rear of the CTD along with a Transition Radiation Detector (TRD). These tracking detectors are positioned within a superconducting coil which provides a high magnetic field of 1.43 $Tesla$ [5]. An Electromagnetic Calorimeter (EMC) and a Hadronic Calorimeter (HAC) surround the coil and provide coverage over the full solid angle. Further still from the interaction point are the muon chambers. Outside of the calorimeters is the Backing Calorimeter (BAC), which measures energy not contained in the calorimeter.

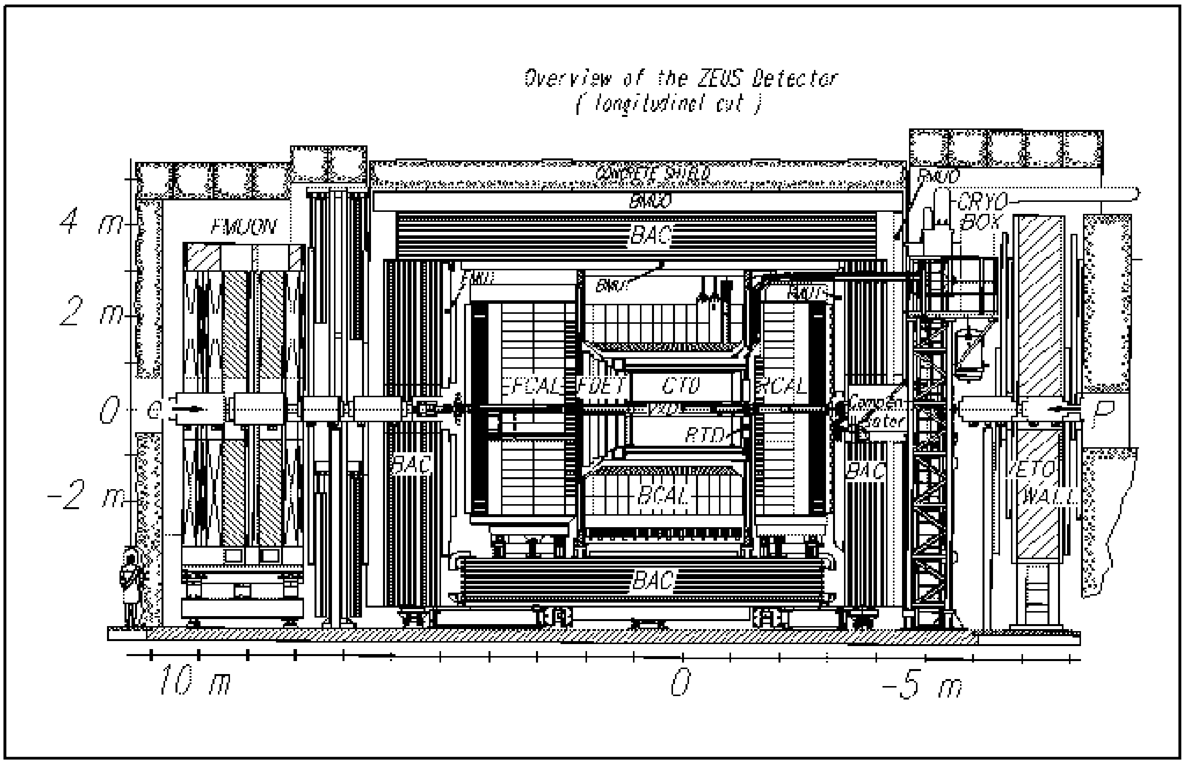

Figure 2: The ZEUS Detector

3.3 Detection of Charged Particles

The inner detectors, consisting of the CTD, FTD and RTD allow the measurement of charged particles over a polar angle range of 7.5° to 170°. The individual elements contribute the following; the CTD provides coverage over polar angles between 15° and 164°; the FTD covers 7.5° to 28°; and the RTD, 160° to 170°. The objectives of the inner detectors are,

- detection of charged particles over a wide range of angle and transverse momentum,
- measurement of charged particles with good momentum resolution,
- particle identification using dE/dx measurements and the TRD,
- reconstruction of tracks from short-lived particle decays,
- fast event triggering,
- measurement of the event vertex by the CTD.

4 The Central Tracking Detector

4.1 The CTD Outlined

An outline of the CTD and its relevance to the determination of dE/dx will now be given. Again, see [4] for a more detailed account. The CTD is a large volume gas container consisting of a cylindrical wire chamber using nine superlayers containing cells with eight sense wires in a cell; see Fig.(4). Five of the superlayers have wires parallel to the chamber axis and four have small angle stereo giving a total of 4608 wires. The chamber was developed around the use of an argon (Ar), ethane (C_2H_6) mixture of Ar/C_2H_6 : 50/50 bubbled through ethanol. The current gas composition is a mixture of argon, carbon dioxide (CO_2) and ethane bubbled through ethanol with the current percentages, as of 19/09/96, being [6] $Ar/CO_2/C_2H_6$: 85.3/5.3/9.4, which represent typical values for the current running period. The percentages used to obtain the curves in Fig.1 were $Ar/CO_2/C_2H_6$: 82.7/4.8/12.5. The sense wires are an integral part of achieving a good dE/dx measurement. Each cell containing eight sense wires has a surface field controlling the gas gain of the signal, and the drift field controls the velocity and direction of the electron drift. The ionised electrons (from the passage of a charged particle) *shower* close to the sense wire, thereby giving a pulse which is measured and recorded via an electronic read-out.

4.2 Drift Cell Design

Various requirements for the cell design had to be met and are the following,

- equality of surface field on the sense wires with a maximum surface field on the cathode wires of 30 kV/cm,
- minimal electrostatic forces on the sense wires, at least below the effects due to gravity,
- good dE/dx measurements are achieved by constraining most electrons to drift to the sense wires and not to the ground wires,
- electric field uniformity over a mesh of points in the drift volume,
- the shaper wires should provide good shielding between superlayers so that the relative pulse sizes do not change with relative alignment of superlayers in z.

4.3 From Pulses to Hits

The electronic read-out mentioned above is the $r-\phi$ 8-bit FADC (Flash Analogue-to-Digital Converter) system which is connected to all sense wires. As it is an 8-bit system, this only allows measurement of a pulse up to a maximum of 255 ADC counts. Therfore there are hits, the values of which cannot be measured and are called saturated hits, see Fig.(3).

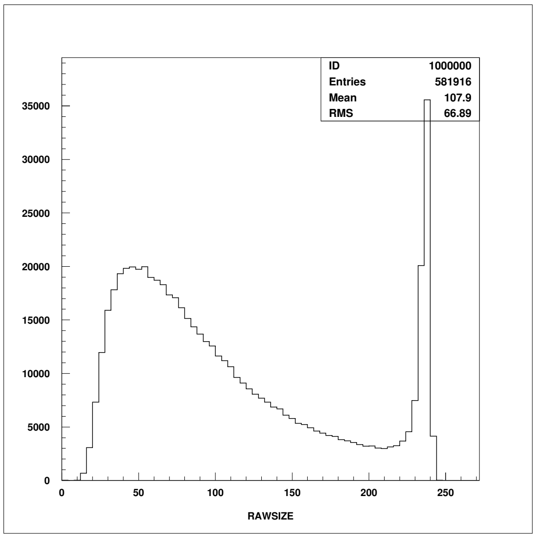

Figure 3: Distribution of Raw Pulse Size

The pulse height is sampled every 9.6 ns, digitised and stored, in order to be analysed by the first-level trigger. The pulse height is then compared with an expected pulse produced via the passage of a charged particle. The pulse height is then analysed to determine a peak signal which gives a measure of the value of a *hit* in FADC counts.

4.4 dE/dx for a Hit

To get a value of dE/dx for a hit, the raw pulse size needs to be corrected for several important factors. Hits may also be rejected and these reasons are also detailed below.

Hits are excluded on the grounds that they are outside understood regions of drift velocity and drift in the z-direction. Hits are also excluded if the hits on the wires have 'bad gains'. 'Bad gains' occur when the gain cannot be determined due to dead or ringing wires. Dead wires are so-called because they give little or no signal. Ringing wires can cause, for example, the the same pulse to be continuously recorded for each hit. Mismeasurement of a hit can occur when the hit is at the edge of a cell or close to wires, where there is a non-uniform electric field. Multiple hits, two or more, on the same wire can similarly lead to a poorly measured value. The raw pulse size needs to be corrected for path length in the cell, particularly for polar angle, superlayer and wire-to-wire differences.

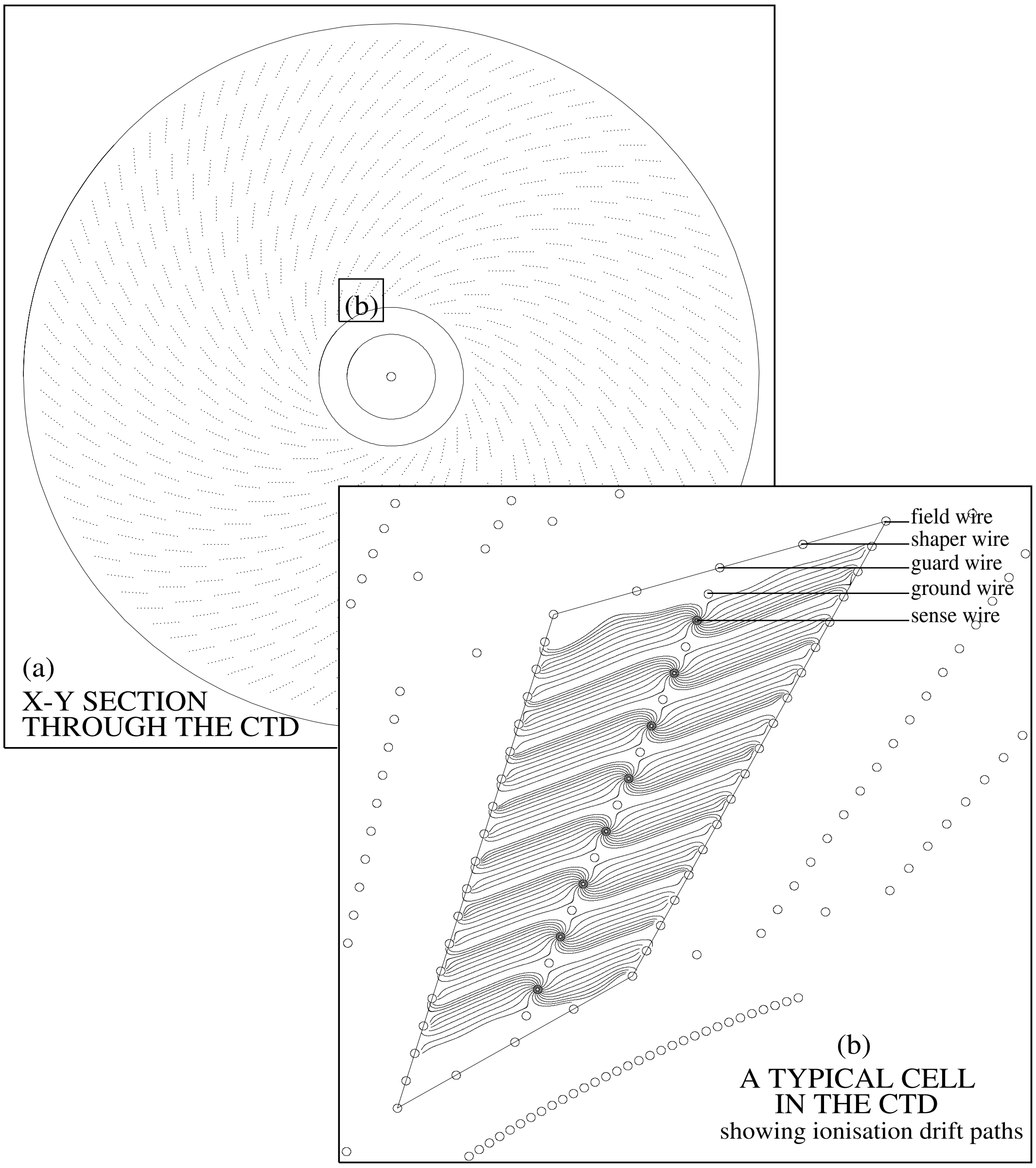

Figure 4: (a) $r - \phi$ cross-section through the CTD, showing the nine superlayers. (b) A representation of a single cell.

5 Finding the Mean dE/dx for a Particle Track

5.1 Introduction to Calculating the Mean

Every hit in a superlayer for a given track gives an energy loss measurement. The corrected pulse sizes are averaged to find a mean energy loss for the particle. Ionization energy loss has a typical Landau distribution. Therefore, to enable the fitting of a Gaussian to the distribution to be a meaningful concept it is desirable to reduce the size of the Landau tail. As well as wanting to reduce the Landau tail, the separation of pions from electrons is also a major consideration. This remains difficult as the average pion energy loss is about 50 ADC counts and electrons have a momentum independent value of 60-65 ADC counts. By looking at different ways of calculating the mean, it was hoped that the resolution of dE/dx could be improved such that pion and electron distinction is possible. The resolution of the Gaussian distribution is given simply by,

$$Resolution = \frac{Sigma}{Mean} \tag{5}$$

and is studied carefully in evaluating the different methods of determining the mean.

The following ways were investigated; the *truncated mean*; the *median*; the *geometric mean*; the *harmonic mean*; and the *variable truncated mean*. To compare these different ways of calculating the mean, each was tested on a 1000 event data sample from run 11593 (in 1995). The minimum number of hits in a track for the mean to be calculated was ten. The mean value of dE/dx was also Bethe-Bloch corrected which means is was normalised to the theoretical value of dE/dx for a pion, as predicted by the Bethe-Bloch equation. This is symbolically represented in the following way: for an uncorrected dE/dx value, dE/dx_{uncorr}, the corrected value, dE/dx_{corr}, is given by,

$$dE/dx_{corr} = \frac{dE/dx_{uncorr}}{BBPi} \tag{6}$$

where $BBPi$ is the predicted Bethe-Bloch value for a pion. To obtain 'quality tracks', a cut of $momemtum > 0.15$ GeV was also applied, i.e. those which are non-highly ionizing. As well as this momentum cut, when looking at how dE/dx varies with polar angle, θ and the number of hits on a track another constraint is applied. This, similarly, is to obtain 'quality tracks' which are non-highly ionizing. This cut was that $(dE/dx)/(BBPi) < 60$ ADC counts.

During the following comparisons of the calculation of the mean, in assessing their relative merits four diagrams will be considered in particular, for each method. These diagrams (see for example, Fig.(5)) will show how dE/dx varies with (a) polar angle, θ, and (b) the number of hits on a track. The values plotted are the mean values of dE/dx and its root mean square for each bin in the value of the abscissa. The dE/dx value of a track should be dependent only on the mass and momentum of the particle, so there should be no dependence on θ or number of hits. If there is some dependence in these plots then this is an indication of problems with the method. (c) shows the dE/dx distribution for all tracks from which the final resolution is calculated. The shape also shows to what extent there is electron-pion separation. The Gaussian fit is the fit that gives the best resolution for each individual method whilst covering at least half of the peak height on the high side of the peak. (d) shows the resolution as a function of cumulative hits in a track. The abscissa is in terms of number of hits on a track, such that the resolution value for a certain value of 'cumulative hits on track' is for all tracks with less than and equal to that number of hits.

5.2 The Truncated Mean

The method of finding the truncated mean [7] is the method that has previously been used to find the average value of dE/dx for a track, due to its associated Landau tail. This is a very simple method of calculation and will now be explained.

The corrected pulse sizes are ordered in ascending value. A 60% mean of these values is then taken by discarding the highest 30% of the hits on the track and the lowest 10% of the hits. As was said in the introduction, the minimum number of hits on a track required for the calculation to be performed is ten *after* truncation, so any given track will require a minimum of sixteen hits. The conventional arithmetic mean of these 'truncated hits' (which form the 60% undiscarded) is then taken and a value of dE/dx is realised in ADC counts for a track. The importance of taking a truncated sample can clearly be seen by comparing Figs.(5) and (6). Fig.(5) shows the effects of using the standard arithmetic mean of all hits. The values plotted in Fig.(5c) are clearly swamped by saturated values and, as a result, give a mean dE/dx of about 70 ADC counts, which is much larger than the expected 50 ADC counts for the pion. The pion and electron separation is therefore also poor as the values for the electrons will be contained within the peak.

As can be seen from Fig.(6) the truncated mean greatly improves the measurement. There is less dependence on θ and number of hits on a track. The distribution is more Gaussian and the mean value is about 50 ADC counts. The final resolution for all tracks is about (11-12)%, which is generally about the best value achieved with this method.

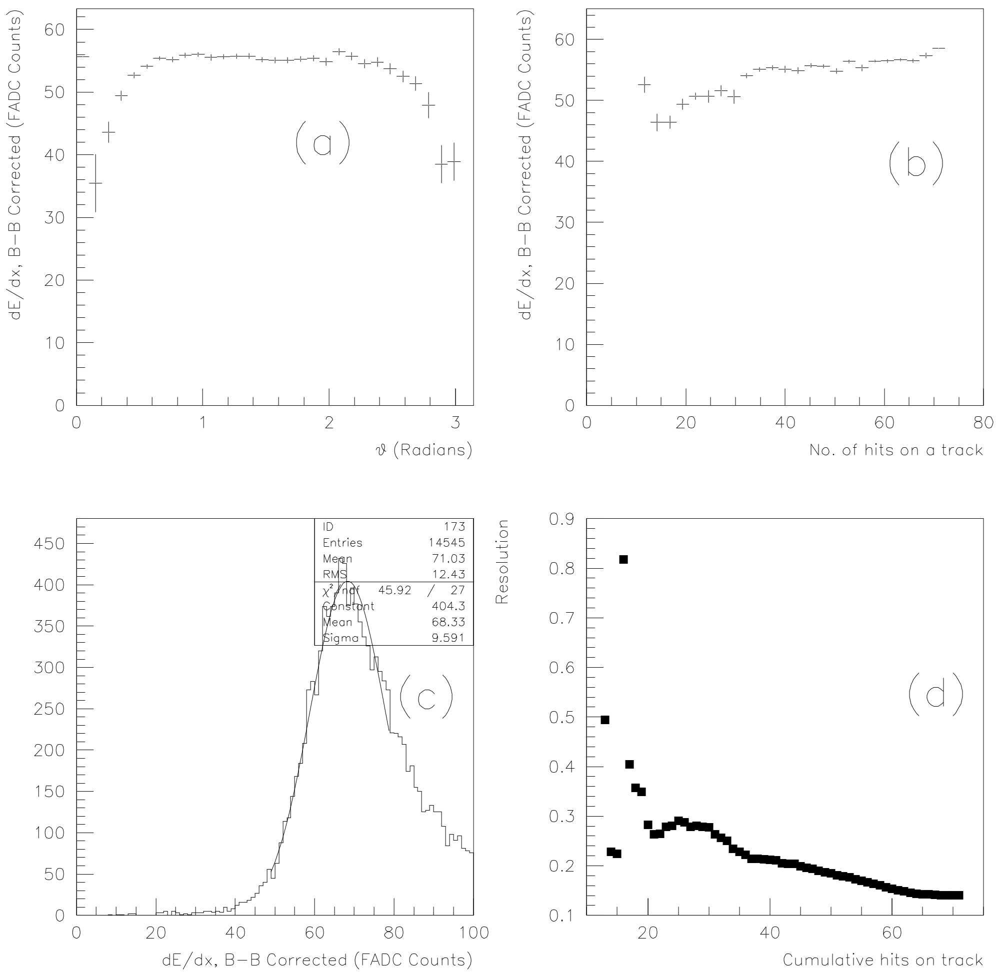

Figure 5: Four diagrams showing the effects of calculating the mean dE/dx with no truncation. The variation of corrected dE/dx is shown with (a) polar angle, θ and (b) number of hits on a track. (c) A Gaussian fit to all the data. (d) Resolution of Gaussian fit as a function of hits on a track.

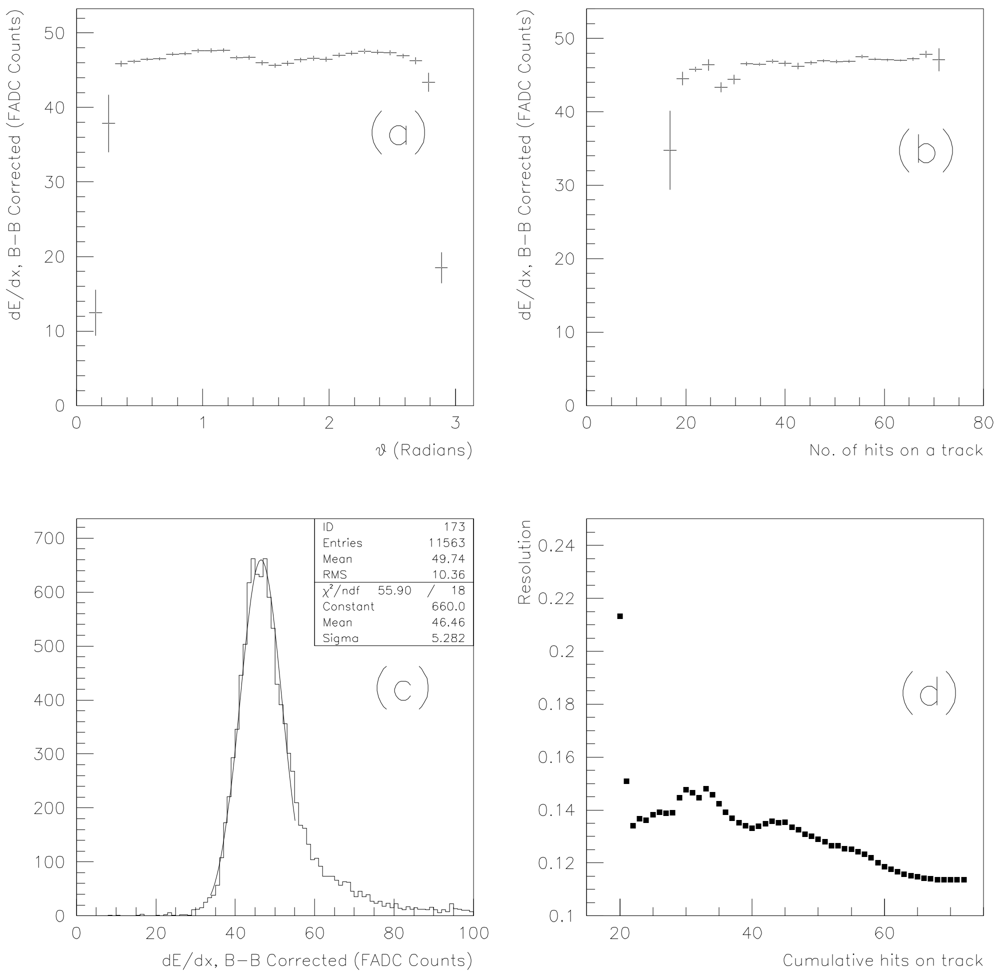

Figure 6: Four diagrams showing the effects of calculating dE/dx via the truncated mean. The variation of corrected dE/dx is shown with (a) polar angle, θ and (b) number of hits on a track. (c) A Gaussian fit to all the data. (d) Resolution of Gaussian fit as a function of hits on a track.

5.3 The Median

The median was calculated by again ordering all the values in ascending order and then taking the central value; the definition of the median. For an odd number of values, the central value is easily defined, but for an even number of values this is less transparent. When there are an even number of values, there are two 'central values', so an average of these is taken. No truncation was involved as the concept of a truncated median is not so well defined.

As can be seen from Fig.(7), the median does not perform very well. Like the mean with no truncation there seems to be a trend towards larger dE/dx for an increasing number of hits on a track. The resolution values are not as good as for the truncated mean with the resolution for all tracks being about 13%, being only one percent better than the untruncated mean. The median seems to be a poor way of calculating the dE/dx of a track and is not good enough to succeed the truncated mean. Perhaps the concept of truncation could be incorporated into the median calculation.

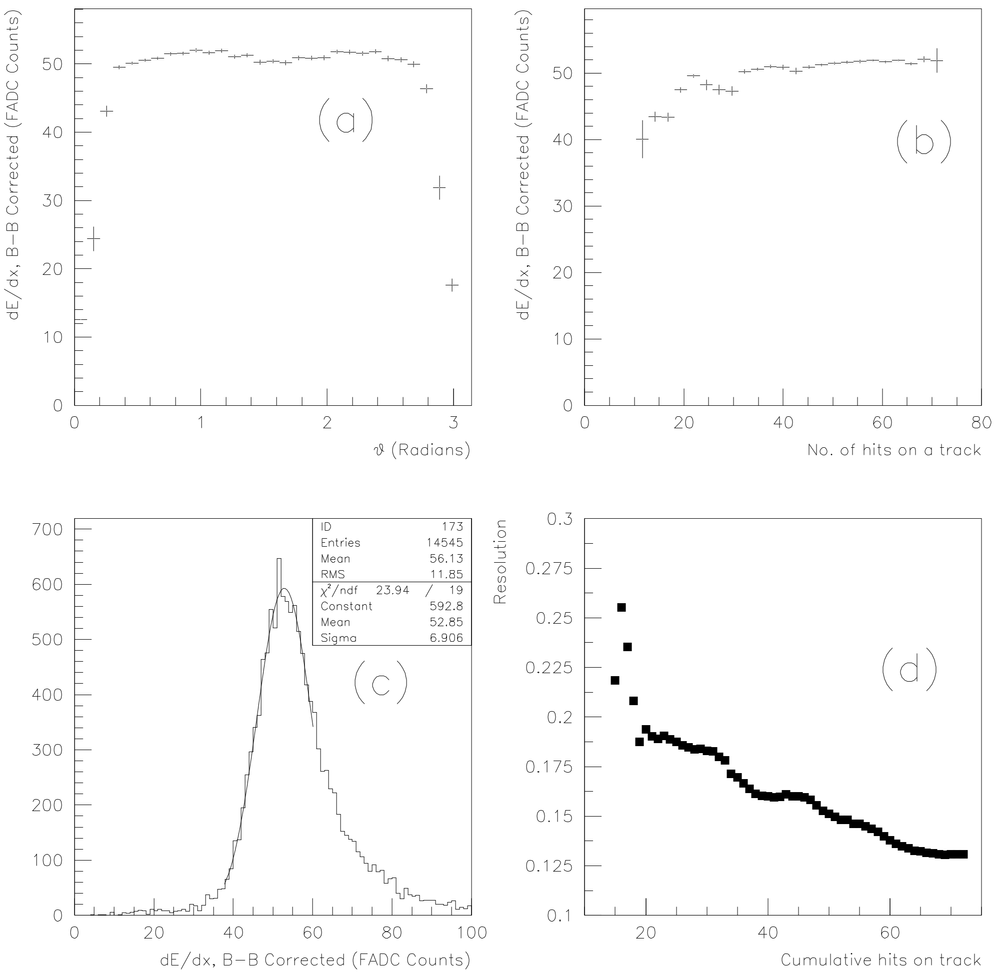

Figure 7: Four diagrams showing the effects of calculating dE/dx via the median. The variation of corrected dE/dx is shown with (a) polar angle, θ and (b) number of hits on a track. (c) A Gaussian fit to all the data. (d) Resolution of Gaussian fit as a function of hits on a track.

5.4 The Geometric Mean

The geometric mean calculation is also a truncated mean method being achieved in the same way as the truncated mean, thereby taking a 60% mean of the undiscarded hits. The geometric mean, $\overline{x_g}$, of a sample of n values is given by the expression [8],

$$\overline{x_g} = \sqrt[n]{\prod_{i=1}^{n} x_i} \tag{7}$$

The idea behind the geometric mean is the fact that it gives less bias to large values. This therefore means the saturated hits have less effect. With this it was hoped that there would be less of a 'bump' around 60 ADC counts (due to electrons) and there would be more of a tail on the other side of the peak. This would have indicated better electron-pion separartion. This has not occurred, with the tails of the truncated and geometric means being of similar magnitude.

The geometric mean, as can be seen in Fig.(8), gives an average value for all tracks that is two ADC counts less than for the truncated mean, due to its bias towards lower values. For all lengths of tracks the resolutions are similar at about (11-16)% except for very short tracks where there are low statistics.

5.5 The Harmonic Mean

The harmonic mean calculation also involved truncation, where the harmonic mean was taken of the 60% undiscarded hits. For n values contributing to the calculation, the harmonic mean, $\overline{x_h}$, is given by, (again see [8])

$$\overline{x_h} = \frac{n}{\sum_{i=1}^{n} 1/x_i}. \tag{8}$$

Similarly as for the geometric mean, the harmonic mean gives less bias to high values, hence the low average value for dE/dx, for all tracks, of 42.65 ADC counts. Also, analogous to the geometric mean calculation, the shape of the distribution see Fig.(9) is similar to the truncated mean, thereby achieving electron-pion separaration which is no better. The resolutions are also of the same order.

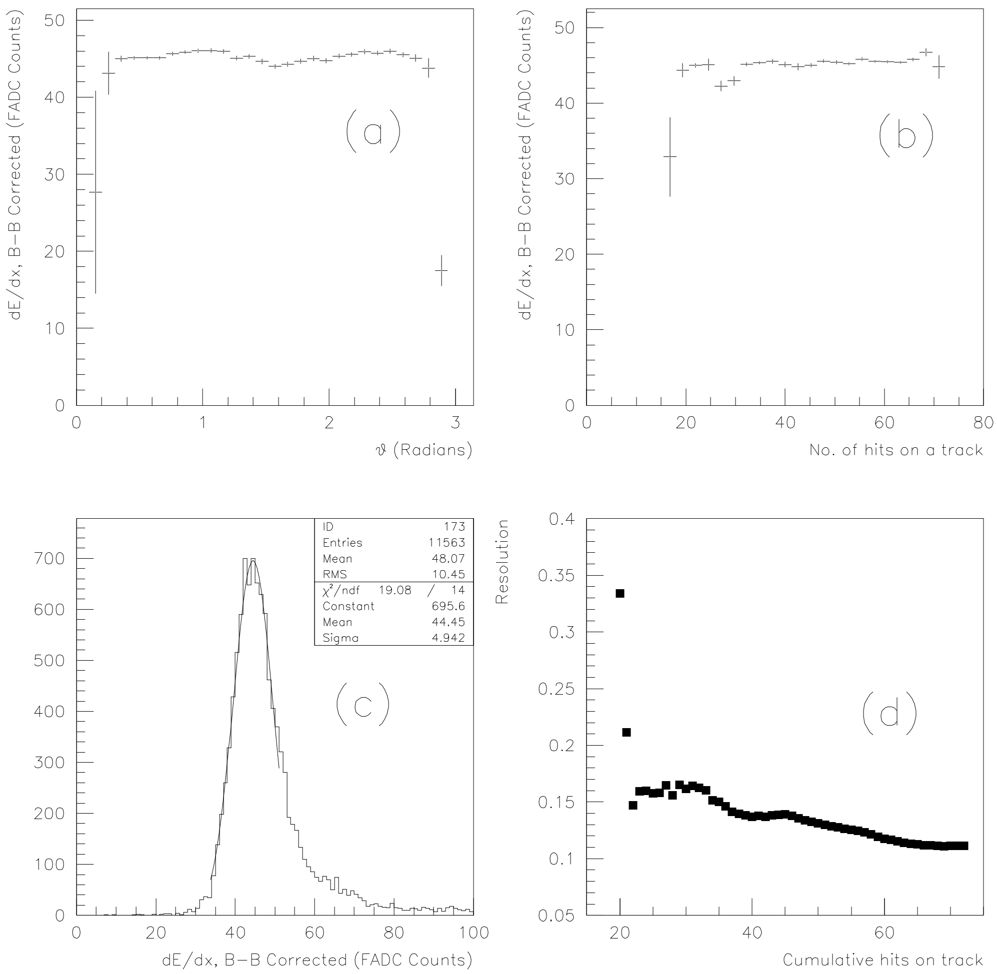

Figure 8: Four diagrams showing the effects of calculating dE/dx via the geometric mean. The variation of corrected dE/dx is shown with (a) polar angle, θ and (b) number of hits on a track. (c) A Gaussian fit to all the data. (d) Resolution of Gaussian fit as a function of hits on a track.

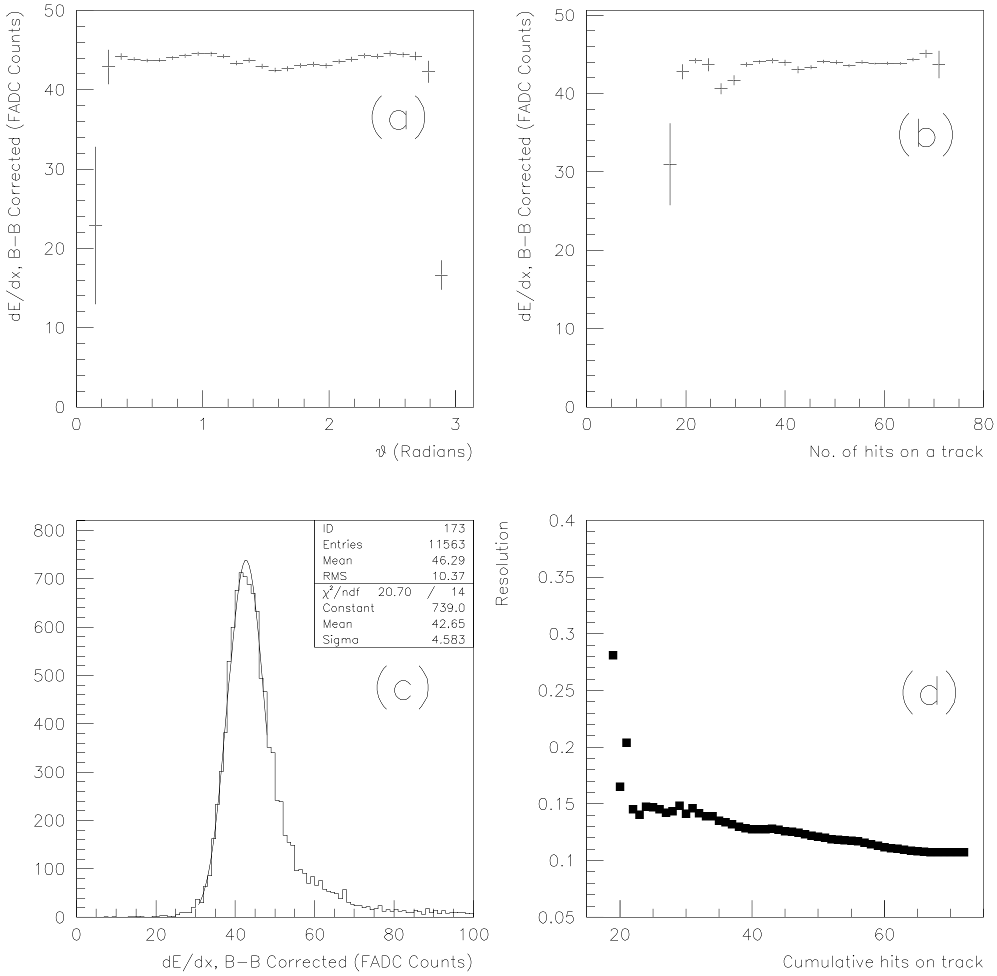

Figure 9: Four diagrams showing the effects of calculating dE/dx via the harmonic mean. The variation of corrected dE/dx is shown with (a) polar angle, θ and (b) number of hits on a track. (c) A Gaussian fit to all the data. (d) Resolution of Gaussian fit as a function of hits on a track.

5.6 The Variable Truncated Mean

The variable truncated mean takes into account the number of saturated hits in the track. Therefore it does not have a rigid truncation of (10-70)% of hits. When the percentage of saturated hits is less than 30% then the 'old' truncated mean method is used as all saturated hits are obviously eliminated. When the percentage of saturated hits is greater than 30% then in previous methods saturated hits are included in the calculation. It is desirable not to have these saturated hits in the calculation, so the variable truncated mean method eliminates them. This is done simply by, instead of eliminating the upper 30% of hits, but eliminating the percentage of saturated hits. Now the 'window' instead of being (10-70)%, is (10-(100-saturated percentage))%. This obviously means that the number of hits used in this case is less than would have been used in the usual truncated mean case. Therefore the value of dE/dx found needs to be normalised upwards by a simple correction factor. The rise of dE/dx with percentage of sample used follows a linear progression. Therefore by plotting dE/dx against the percentage of hits used and performing a least squares fit on the points, the gradient and intercept of the curve are trivially found and hence the normalised value.

As can be seen from the Fig.(10), the variable truncated mean has very little affect on the resolution or electron-pion separation already established by the truncated mean. This is because almost all the tracks which used the variable truncated mean had a large value of mean dE/dx. By this method the value was reduced but it was a reduction of a value of the order of 200 to a value of the order of 160. Therefore these were nearly all outside the range of the peak and consequently are insignificant. It has been found by Wouter Verkerke [9] that the variable truncated mean does work well and give better resolutions for tracks with a relatively small number of hits. The reason there is no real difference seen here may be due to a lack of statistics.

Within the CTD the number of hits on a track and the number of saturted hits are strongly anti-correlated. This is due to short CTD tracks, which leave through the end plates, having a long ionization path length past each sense wire. This then means that these tracks give bigger pulses. Therefore to eliminate this effect, each track is chosen to be of the same length by randomly discarding hits and then recalculating the value of dE/dx.

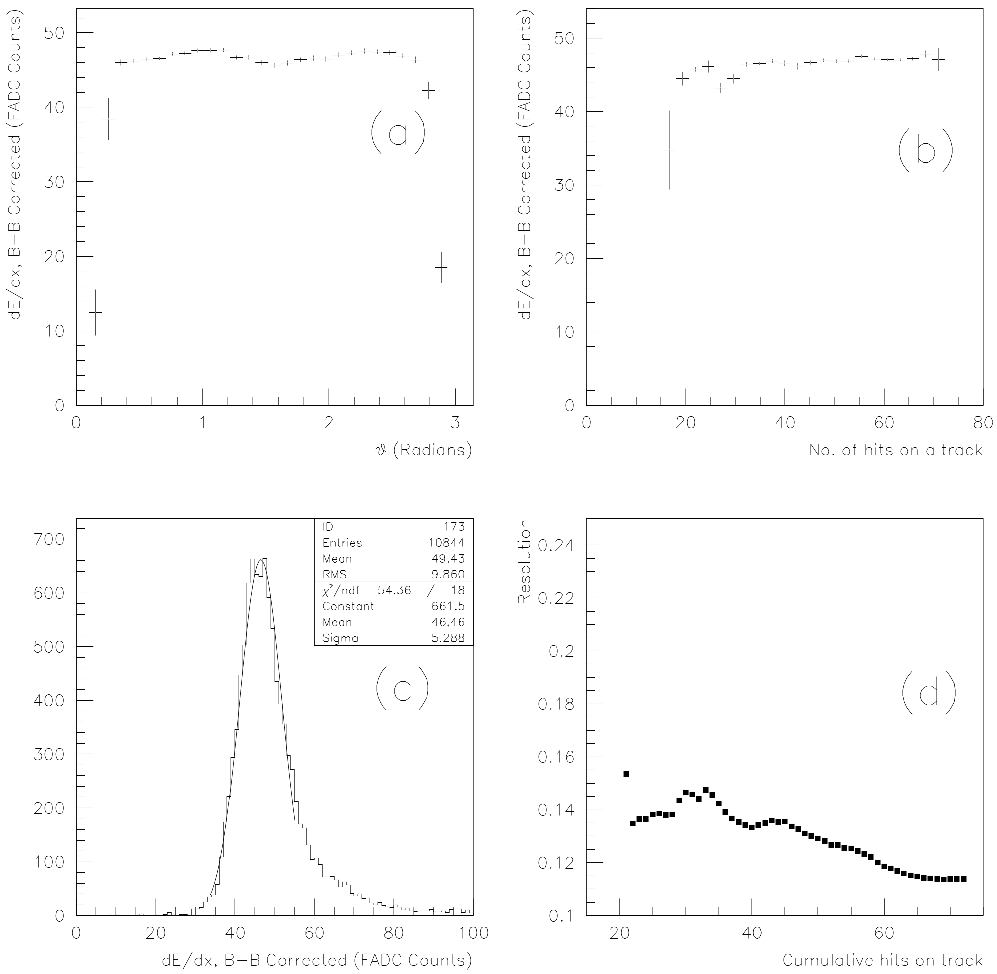

Figure 10: Four diagrams showing the effects of calculating dE/dx via the variable truncated mean. The variation of corrected dE/dx is shown with (a) polar angle, θ and (b) number of hits on a track. (c) A Gaussian fit to all the data. (d) Resolution of Gaussian fit as a function of hits on a track.

It was required that each track have 54 or more hits and those with greater than 54 were reduced to the same value. The value of dE/dx was then calculated for tracks (all of which had greater than or equal to 54 hits) for 54 hits and down to the minimum number of hits, 16. By doing this it is possible to investigate the relationship of the resolution of dE/dx with "pure" hits. The resolution should follow a $1/\sqrt{N_p}$ curve, where N_p is the number of pure hits. As can be seen from Fig.(11), the resolution of the variable truncated mean does become improved with 'pure' hits. Wouter Verkerke found that for the short tracks, the values were closer to these "pure" values than was the case for the truncated mean. He considers this promising.

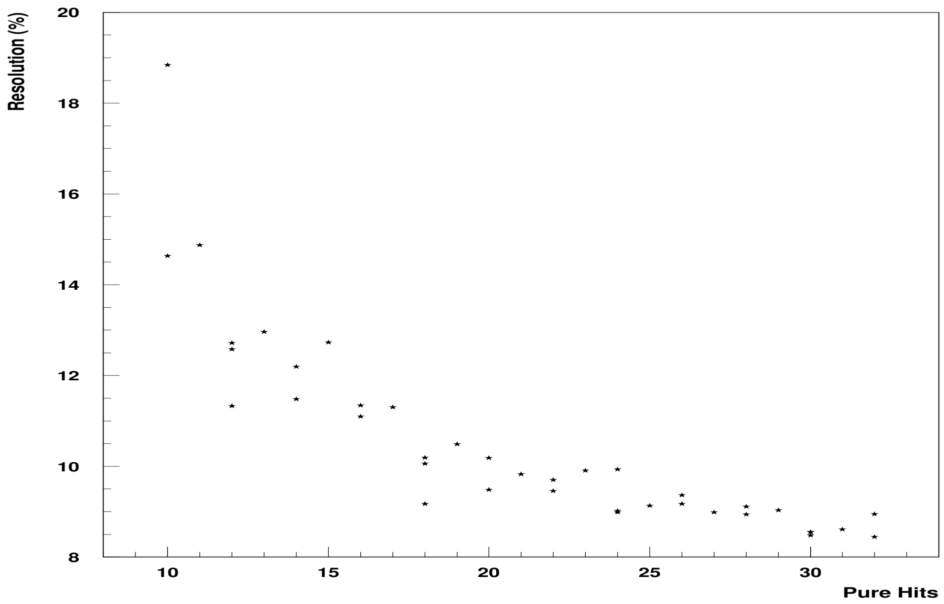

Figure 11: The resolution as a function of pure hits for the truncated mean.

5.7 Concluding Remarks

The investigation into different ways of calculating the mean was not significantly conclusive. Other methods that were considered did not produce better results than the already established truncated mean method. There was no one outstanding candidate.

The original investigation was into the median method which proved to be unpromising except perhaps if truncation was incorporated. The additional methods, although not thoroughly investigated, yielded similar results. These could be investigated further by investigating various adaptations such as variable range truncation and using higher statistics so tighter cuts could be made on polar angle and momentum, for example.

6 Pressure Corrections to dE/dx

6.1 External Factors Affecting dE/dx

As mentioned previously, the major factor affecting the value of dE/dx is the pressure variation which thereby changes the gas density. This variation in gas density has a direct consequence on the average pulse size. Over the running period during 1995 the pressure variation was up to 50 mBar in 1000 mBar; see Fig.(12). This is a significant amount.

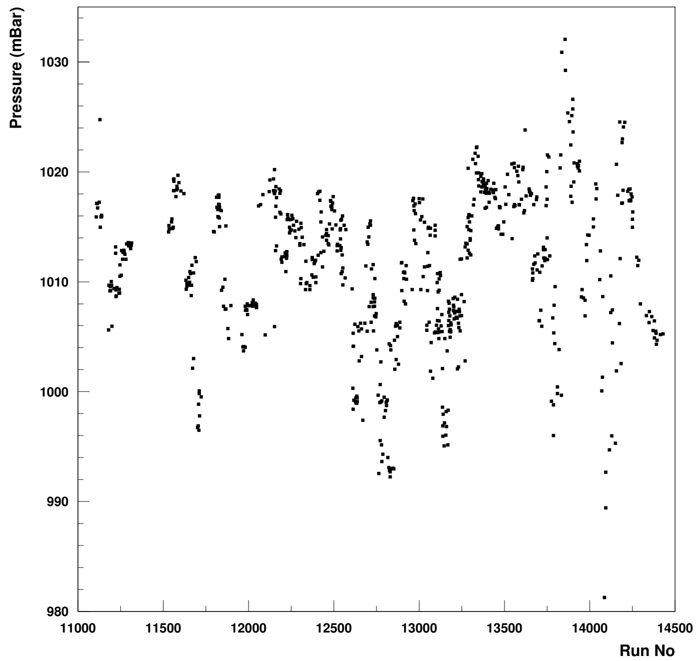

Figure 12: Pressure variation with run in 1995.

A measure of the drift velocity and Lorentz angle (the angle between the electric field lines and drift direction) indicate changes in the gas composition and hence in the pulse sizes.

High voltage changes cause a variation in signal amplification. This is kept very stable, so is not generally a feature that needs to be taken into account.

6.2 The Pressure Corrections

By choosing to determine the average dE/dx for pions around the minimum ionization one can set a scale for the run. They are chosen to be a minimum ionizing particle (mip), i.e. a pion in the momentum range 0.3 to 0.4 GeV/c, as at these momenta pions are more easily distinguishable from other particles. At this momentum range a clear pion signal is achieved.

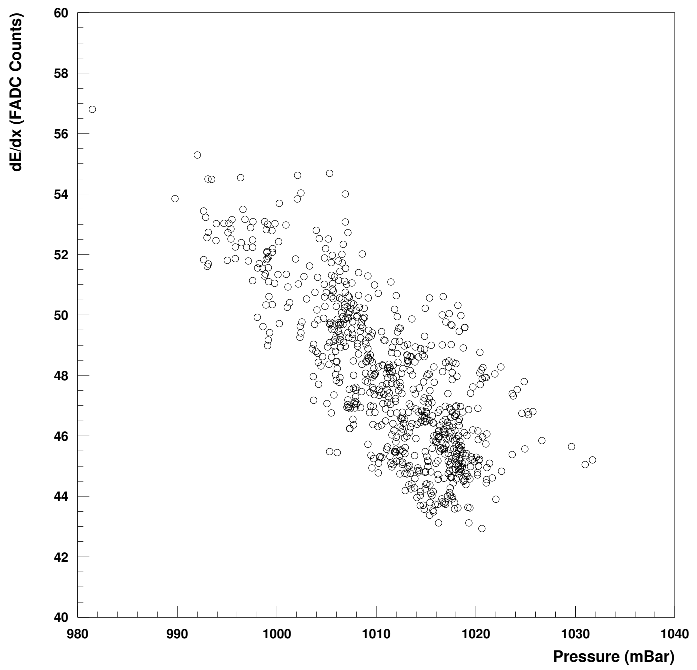

Figure 13: dE/dx correlation with pressure.

The pressure was recorded (in 1995) about every ten minutes and stored in data files. An average pressure for a particular run can then be found and the variation of the average dE/dx with average pressure can be seen in Fig.(13). As can be seen, the variation is linear, with the spread being due to the other factors previously mentioned. Therefore, by normalising the value of dE/dx to a pressure of 1013 mBar one can eliminate the pressure effects. Fig.(14) shows the result of correcting for pressure. This should be a spread of points (with no particular slope) around a value of one. However there does seem to be a trend, with a general downward slope to and a general upward slope from about run 12250.

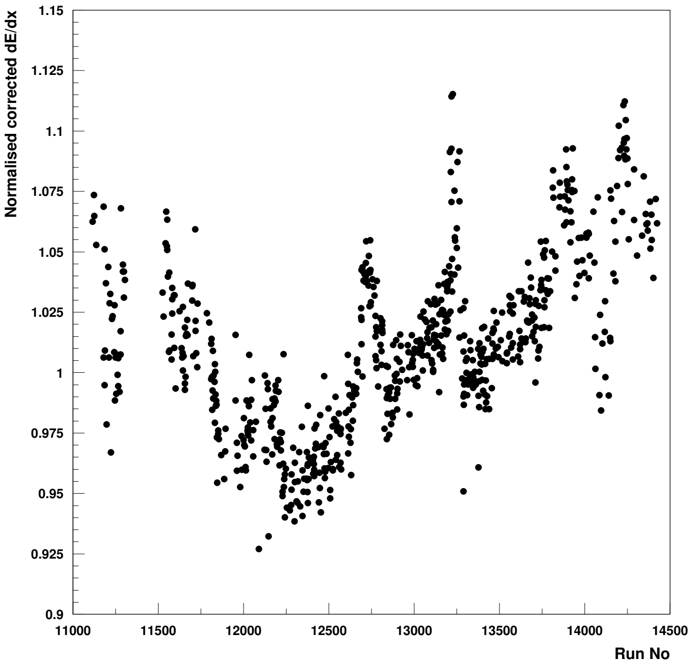

Figure 14: The pressure corrected values of dE/dx against run.

This appears to be due to changes in the drift velocity. Inspection of Fig.(15a) along with the corrected dE/dx indicates an anti-correlation between corrected dE/dx and drift velocity, such that with decreasing drift velocity there is increasing corrected dE/dx and vice versa. Although this explains the trend seen, the reason behind the change in drift velocity is not known. It is thought that this variation in drift velocity would be reflected in a similar way in the variation of the Lorentz angle as they are both a reflection of the properties of the gas. This variation is less marked in the history of the Lorentz angle (Fig.(15b)) but is consistent and the reason is not understood at present.

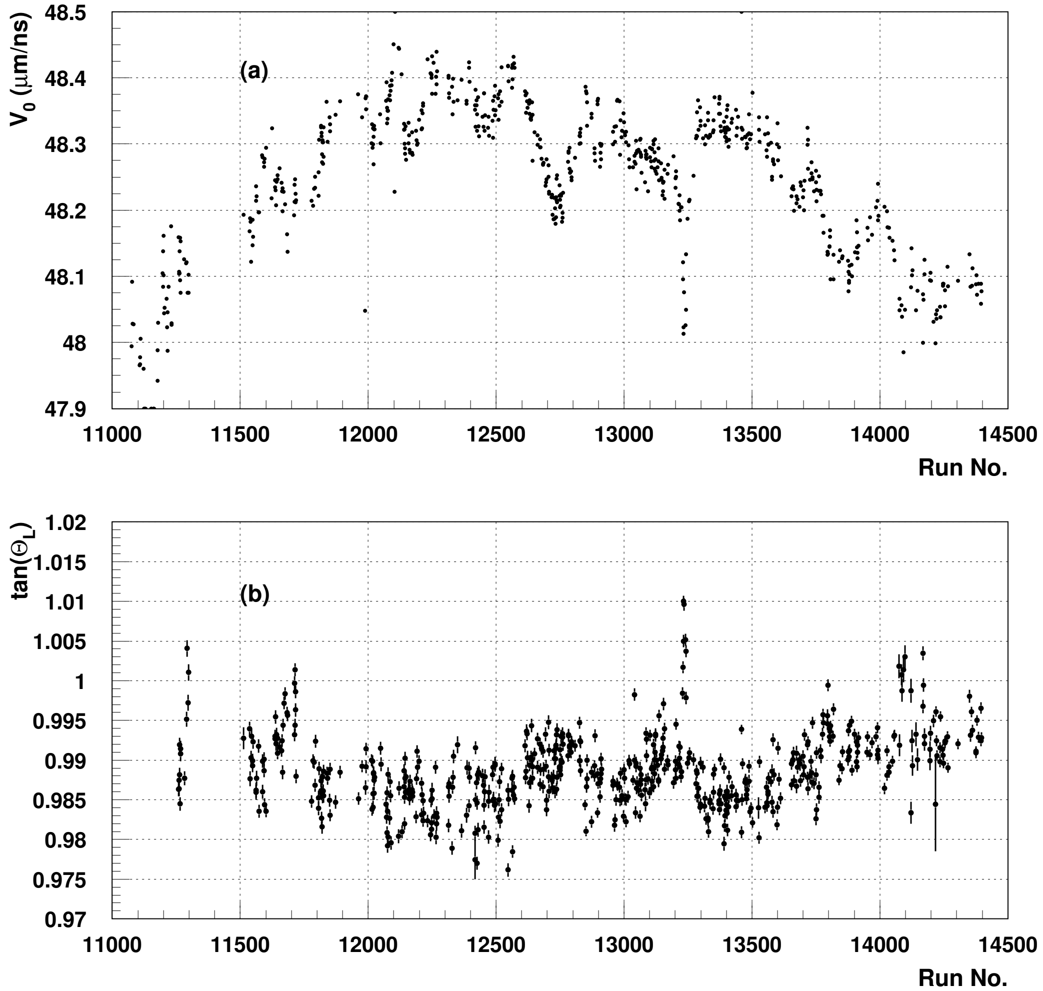

Figure 15: History plots of (a) drift velocity against run number and (b) Lorentz angle against run number.

6.3 How the Corrected dE/dx Values have been used in Analyses

In the neutral current deep inelastic scattering process, $e+p \rightarrow e+X$, the dominant reaction for the production of charmed quarks is photon gluon fusion (PGF). The major motivation for these studies is to get detailed measurements such that the gluon distribution inside the proton can be measured. This is thought to be predominant over the two other proceesses, namely, diffractive heavy flavour production [10] and scattering off intrinsic charm in the proton [11]. The charm quarks produced may then hadronize into $D^*(2010)$ mesons. The singly charged D^* mesons decay primarily into a D^0 meson and a pion. The branching ratio for the decay is $(68.3 \pm 1.4)\%$ [12]. There are two other decay channels for the $D^*(2010)$ meson; the decay into a $D^{\pm}$ and a neutral pion with a branching ratio of $(30.6 \pm 2.5)\%$ [12]; and with a branching ratio of $(1.1 \pm {}^{2.1}_{0.7})\%$ [12] the decay into a $D^{\pm}$ and a photon. The resultant D^0 has many decay channels. The two specifically looked at which used the dE/dx corrections were:

$$D^{*+} \rightarrow D^0 + \pi_s^+ \rightarrow K^- + \pi^+ (+\pi_s^+)(+c.c.)^2 \tag{9}$$

and

$$D^{*+} \rightarrow D^0 + \pi_s^+ \rightarrow K^- + \pi^+ + \pi^- + \pi^+ (+\pi_s^+)(+c.c.) \tag{10}$$

where the "s" denotes the "slow" pion as the $Q-value$ for the reaction $D^* \rightarrow D^0 \pi_s$ is very small, such that the D^0 and π_s are almost (but not quite) produced at rest in the D^* center-of-mass frame. The resulting kaons and pions can be detected and invariant mass combinations of tracks for the D^* and D^0 can be formed. The combination,

$$\Delta M = M(D^0 \pi_s) - M(D^0) \tag{11}$$

can be measured with better precision than the D^* mass itself.

The use of dE/dx is obvious in that it can be used to distinguish the resulting kaons and pions particularly the 'soft' pion. The use of dE/dx improves the signal to background ratio of the ΔM distribution. This measurement enables the ep cross-section for the production of D^* mesons to be determined and compared with QCD calculations.

[2] The charge conjugate reactions have the same branching ratios as those for the ones given.

7 Photoproduction and Future Plans

7.1 Photoproduction

At Leading Order (LO), hard photoproduction [13] (production of an almost real ($Q^2 \approx 0$) photon, with an additional hard scale such as the observation of a high transverse energy, E_T, jet) has two contributions, "direct" and "resolved". The direct process (see Fig.(16)) is where the photon couples in the hard sub-process directly with all its momentum, interacting with a gluon (PGF) or a quark (QCD Compton). The resolved process (see Fig.(17)) is such that the photon is assumed to fluctuate into a hadronic state. It is therefore the partonic constituents of the photon which interact in the hard sub-process with some fraction of the photon momentum. In Next to Leading Order (NLO) calculations (the more realistic case) the direct and resolved processes are not clearly defined. In LO, there are two jets in the final state, NLO allows for the possibility of more than two jets and non-zero components of transverse energy for the photon and proton remnants.

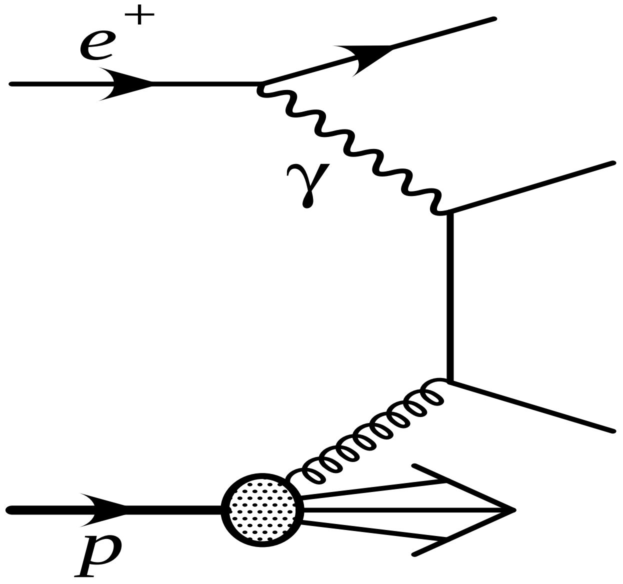

Figure 16: Direct photoproduction.

Experimentally, what indicates the process is photoproduction at ZEUS is the absence of a scattered electron in the uranium calorimeter indicating a low

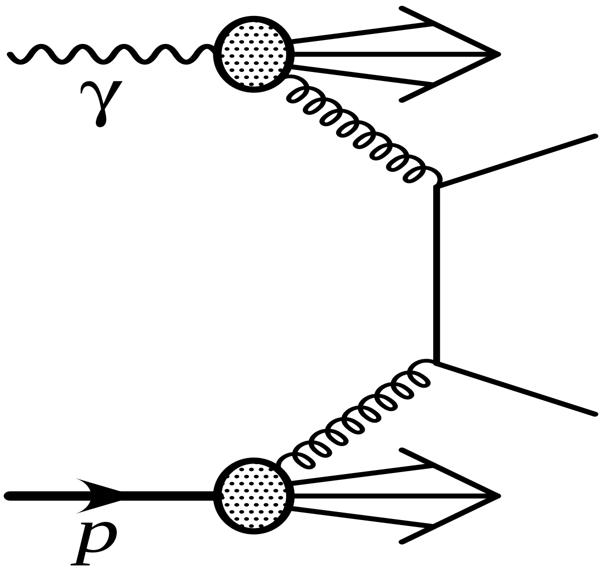

Figure 17: Resolved photoproduction.

scattering angle and hence low scale, Q^2. When there are large values of transverse energy in the final hadronic state and no missing transverse energy, then the process is termed hard photoproduction.

7.2 Future Plans

The analysis of charm production via these photoproduction processes is something being studied. The decay channels in equations (9) and (10) are being studied currently within ZEUS. In an analagous sense to DIS the photoproduction analysis makes use of dE/dx measurements thereby distinguishing the pions from the kaons in the processes (9) and (10).

The use of dE/dx measurements and its ability to distinguish particles is going to be incorporated into the analysis of the semi-leptonic decay channels of the D^0 meson. The two decays with the largest branching ratios and hence of great interest are,

$$D^{*+} \rightarrow D^0 + \pi_s^+ \rightarrow K^- + e^+ + \nu_e(+\pi_s^+)(+c.c.) \tag{12}$$

and,

$$D^{*+} \rightarrow D^0 + \pi_s^+ \rightarrow \overline{K^0} + \pi^- + e^+ + \nu_e(+\pi_s^+)(+c.c.), \qquad (13)$$

with branching ratios of $(3.64 \pm 0.20)\%$ and $(2.8\pm^{1.7}_{0.9})\%$ respectively [12].

By analysing all events which satisfy the above criteria and introducing more specific tighter cuts (to be decided), a sample of possible photoproduction events is found. By then performing jet finding [14] on all cells of the uranium calorimeter using a cone algorithm a set of photoproduction events is then found. The knowledge of the dE/dx values can then be incorporated to identify the electrons and hence the semi-leptonic channels.

There are important physics motivations for studying charmed photoproduction processes. They will provide a direct measurement of the gluon distribution inside the proton. This will be independent, but complimentary to those made in DIS. The charm content of the photon is not known and can be studied via the analysis of these processes. This in turn will give information on the QCD evolution of massive quarks and whether perturbative QCD is applicable at the charm mass scale.

References

[1] B. Rossi; "High-Energy Particles", Prentice-Hall (1952).
B.R. Martin and G. Shaw; "Particle Physics", Wiley (1992).

[2] H.A. Bethe; Annalen d. Physik **5** (1930) 325.
H.A. Bethe; Zeits. f. Phys. **76** (1932) 293.

[3] G.C. Wick; Ricera Scient. **12** (1941) 858.
G.C. Wick; Nuovo Cim. **1** (1943) 302.
O. Halpern and H. Hall; Phys. Rev. **73** (1948) 477.

[4] ZEUS Collab.; The ZEUS Detector, Status Report (1993).
C. Catterall; PhD. Thesis "Measurement of charged particles from the hadronic final state of electron-proton deep inelastic scattering at a centre of mass energy of 296 GeV", University College London (1995).

[5] ZEUS Collab.; "Dijet Angular Distributions in Direct and Resolved Photoproduction at HERA", DESY 96-094.

[6] M.R. Sutton; "Status of ZEUS CTD Gas System" WWW currently
`http://www-zeus.desy.de/ sutt/gas/gasnow.html`

[7] W.W.M. Allison and P.R.S. Wright; "The Physics of Charged Particle Identification: dE/dx, Cerenkov and Transition Radiation", in: Th. Ferbel; "Experimental Techniques in High-Energy Nuclear and Particle Physics", 2^{nd} Ed., World Scientific (1991).
W.W.M. Allison and J.H. Cobb; "Relativistic Charged Particle Identification by Energy-Loss", Ann. Rev. Nucl. Part. Sci. **30** (1980) 253.

[8] R.J. Barlow; "Statistics", Wiley (1989).

[9] W. Verkerke; dE/dx Minutes (pre-release) (1996)

[10] K. Goulianos; Phys. Rep. **101** (1983) 169.
P. Bruni, G. Ingelman and A. Solano; Proceedings of the workshop "Physics at HERA" vol.1, DESY (1992) 363.

[11] S.J. Brodsky et al.; Phys. Lett. **B93** (1980) 451.
S.J. Brodsky et al.; Nucl. Phys. **B369** (1992) 519.
G. Ingelman, L. Jönsoon and M. Nyberg; Phys. Rev. **D47** (1993) 4872.

[12] Review of Particle Physics; Phys. Rev. **D54** (1996).

[13] R.G. Feild; PhD. Thesis "Jet Photproduction and QCD at HERA", The Pennsylvania State University (1995).
M. Drees and R.M. Godbole; "Resolved Photon Processes", hep-ph/9508221 (1995).

[14] ZEUS Collab.; Phys. Lett. B **348** (1995) 665.